2013 European Control Conference (ECC)
July 17-19, 2013, Zürich, Switzerland.

Robust Control of Flexible High-Speed Rotors via Mixed Uncertainties

Bernd Riemann, Martin A. Sehr, Rudolf Sebastian Schittenhelm, and Stephan Rinderknecht

Abstract— **Active vibration control for flexible high-speed rotors tends to be a particularly challenging problem due to the influence of gyroscopic terms, resulting in the need for speed-dependent system models. This paper addresses robust control of such systems, using Linear Fractional Transformations (LFTs) for decoupling the system model into speed-dependent and -independent components in LFT feedback. Based on the resulting LFT decomposition, the speed-dependent terms are efficiently reduced in order and considered uncertain with respect to the rotational speed of the shaft. The resulting perturbations are augmented by complex, additive uncertainties and explicitly used for control synthesis. Defining semi-modal performance measures, the perturbed open-loop systems are well-suited for mixed μ synthesis techniques. In particular, (D,G)-K and μ-K algorithm, both enabling explicit treatment of mixed perturbations, are investigated in approaching the robust vibration attenuation problem across the range of operating speeds.**

I. INTRODUCTION

Bending vibrations are a limiting factor in design of numerous industrial rotating machineries. For high-speed and high-precision applications, passive methods like balancing or integration of additional damping elements such as squeeze film dampers hit accuracy limits, especially when multiple resonance frequencies of a flexible rotor are within its range of operation. In many such cases, unbalance is the dominating excitation source of bending vibrations [12]. Hence, the issue of active vibration control for flexible rotor systems is investigated by numerous researchers.

Lots of publications on active rotor systems consider rotors supported by active magnetic bearings, as the idea of active vibration control arises naturally in the presence of active bearings [29]. Alternative concepts such as semi-active dampers (e.g. adaptive squeeze film dampers [5]) or active bearings by means of ball bearings supported by piezoelectric stack actuators have been developed in the last decades [20]. The latter option offers advantages in terms of high force generation at low phase lag and relatively low weight. Usually, the actuators are located at the bearings, which are close to the nodes of the lower bending vibration modes, limiting their controllability. Further issues regarding practical applications of piezoelectric stack actuators include hysteresis induced self-heating and demands on operating conditions such as temperature range and load directions [26].

From a control synthesis point of view, the dynamics of high-speed flexible rotors are time variant as gyroscopic terms depend on the shaft's rotational speed. For increasing rotational speeds, the standstill eigenmodes and natural frequencies split up into so-called forward- and backward whirls, while only forward whirl modes are excited by unbalances [12]. Most publications on active rotor systems subject to severe gyroscopic effects deploy linear control techniques, either robust ones or such adaptive with respect to the shaft's rotational speed. Adaptive feedforward control schemes have resulted in remarkable performance, but induce restrictions concerning stability analysis, local vs. global vibration attenuation, and the need for a signal that is correlated with the unbalance [15]. Adaptive feedback designs for high-speed rotors usually employ gain scheduling of Linear Time Invariant (LTI) controllers, as stability and dynamics using direct nonlinear controllers are hard to predict [16]. Special forms of such approaches, partially in combination with robust control techniques, are being developed [17].

Robust control techniques allow the synthesis of controllers yielding guaranteed stability and performance at the cost of increased modeling effort, more involved optimizations, and some design-induced degree of conservatism [21]. New approaches via Linear Matrix Inequality (LMI) methods have been suggested in recent years, for instance such adding robustness to $\mathcal{H}_2$ controllers [6], although applications to high-speed rotors subject to severe gyroscopic effects are rare. Two established robust control techniques are $\mathcal{H}_\infty$ and Structured Singular Value (SSV, μ) synthesis, both utilized successfully for actively reducing vibrations of rotor systems [11], [13]. For flexible high-speed rotors under significant gyroscopic influence, complex μ synthesis via D-K Iterations [8] has been shown to yield solid performance and robustness properties [24]. However, caused by its limitation to complex model perturbations, complex μ synthesis induces significant conservatism. In order to greatly reduce this design-induced conservatism, the gyroscopic influence can be captured using a real parametric uncertainty. Replacing this real perturbation element by complex uncertainties, as done in [17], induces a large degree of conservatism.

In this paper, the real perturbation capturing gyroscopic effects is tackled employing mixed μ synthesis via (D,G)-K [32] and μ-K [27] Iterations, respectively. These approaches allow the explicit inclusion of real perturbations in uncertainty models, promising a non-conservative treatment of flexible high-speed rotors. In section II, the nominal open-loop model of a particular rotor test rig is described,

B. Riemann, R. S. Schittenhelm, and S. Rinderknecht are with the Institute for Mechatronic Systems, TU Darmstadt, Darmstadt, Germany (email: bernd.riemann@gmail.com, schittenhelm@ims.tu-darmstadt.de, rinderknecht@ims.tu-darmstadt.de).

M. A. Sehr was with the Institute for Mechatronic Systems, TU Darmstadt, Darmstadt, Germany. He is now with the Department of Mechanical and Aerospace Engineering, University of California, San Diego, La Jolla, USA (email: msehr@eng.ucsd.edu).

including a brief introduction on rotordynamics. Section III provides a brief survey regarding the control synthesis techniques applied to the perturbed, augmented open-loop plant model introduced in section IV. Ultimately, the closed-loop results are summarized in section V.

II. NOMINAL PLANT MODEL

This section addresses a brief introduction on the dynamics of flexible high-speed rotors, translating into an accurate low-order model of the concrete rotor test rig investigated in this paper.

A. Test Rig

The dynamics of a high-speed flexible rotor system are varying according to the rotational speed Ω of the shaft, captured in the linear equations of motion for the displacements q_i:

$$M\ddot{q} + (D + \Omega G)\dot{q} + Sq = F. \tag{1}$$

While mass matrix M, damping matrix D, and stiffness matrix S are constant symmetric matrices, respectively, the skew-symmetric gyroscopic matrix G is multiplied by Ω. This speed-dependency within the equations of motion results in a shift of the system's natural frequencies. While the gyroscopic matrix is commonly summarized as the product $G^* = \Omega G$, the notation used here translates naturally towards the inclusion of perturbations addressed in section IV. For the remainder of this paper, G shall denote the gyroscopic matrix corresponding with a rotational speed of 1 rad/s.

The considered rotor system is a two disk flexible rotor, supported by a passive and an active piezoelectric bearing. The actual test rig is depicted in fig. 1, the construction of the active bearing being illustrated by fig. 2. The rotor is designed for significant exposure to gyroscopic effects and capability of passing two resonance speeds below the DC motor's maximum speed of approximately 8,000 rpm.

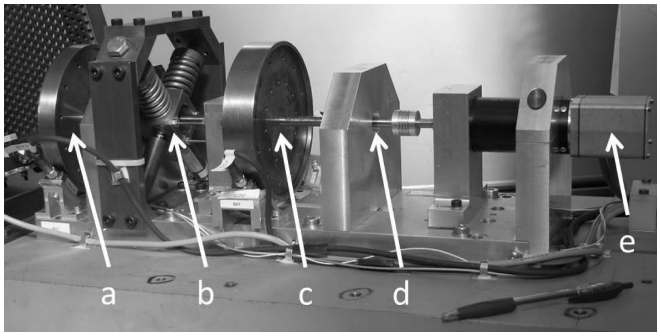

Fig. 1. Test rig: (a) disk 1, (b) active bearing, (c) disk 2, (d) passive bearing, (e) DC-motor

The shift of natural frequencies caused by the skew-symmetric gyroscopic terms in (1) is displayed in fig. 3, employing a Campbell diagram. It can be seen within this diagram how, for increasing rotational speed $\Omega > 0$, each standstill natural frequency splits up into a backward (descending branches) and a forward whirl frequency (ascending branches). Each of these pairs corresponds to eigenforms of similar shape, forward whirl modes rotating in the shaft's direction and backward whirl modes in the opposite direction, respectively. However, for isotropic bearings, unbalance excitation introduces only synchronous forces that rotate in the shaft's direction. Critical rotor speeds are such where the synchronous line (dashed) crosses the natural frequency of forward whirl modes. As backward whirl modes are not excited by the unbalance, there are exactly two critical rotor speeds within the range of operation, at approximately 2,900 rpm and 6,300 rpm, respectively.

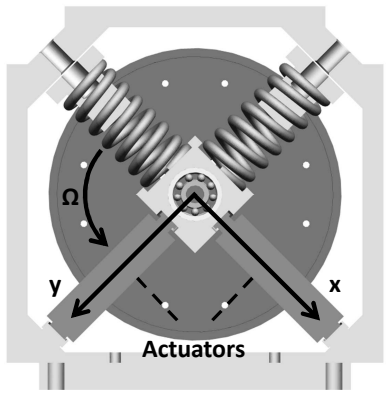

Fig. 2. Active bearing

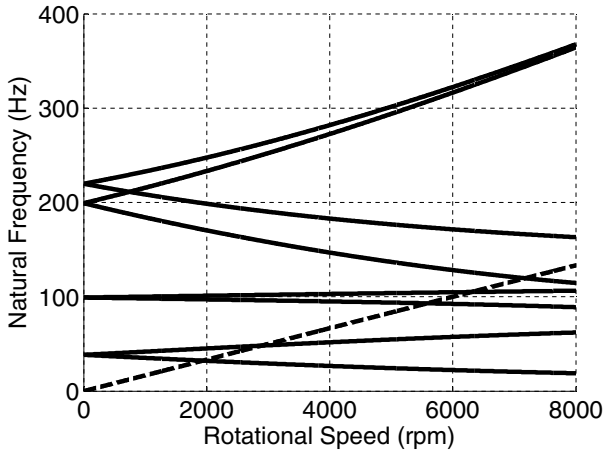

Fig. 3. Campbell diagram: forward and backward whirl natural frequencies (solid), synchronous line (dashed)

B. Modeling

A model yielding high precision within the considered bandwidth is essential for successful control synthesis. For the approach of non-conservative uncertainty tackling suggested below, a model with explicit in- and outputs for capturing gyroscopic effects is required. Such a model allows subsequent LFT decomposition into speed-dependent and speed-independent terms, as depicted in fig. 4. Due to the number of the required in- and outputs, it would not be reasonable to identify such a model via black box identification techniques. Therefore, a theoretical model is generated using Finite Element (FE) modeling, employing Timoshenko beam

elements and stiffness coefficients for the ball bearings. After transforming the equations of motion (1) into a state-space representation

$$\dot{x} = Ax + Bu \quad y = Cx, \tag{2}$$

the piezoelectric stack actuators are included utilizing linear piezoelectric equations in strain-charge form [14]. To increase model accuracy, a modal damping ratio of 0.01 with respect to all considered modes was imposed to fit experimentally identified frequency response functions of the test rig system.

Obviously, the order of the resulting state-space model is twice the number of degrees of freedom captured with the FE model, demanding some model order reduction prior to control synthesis. Modal reduction of the standstill model and subsequent LFT decomposition as shown in fig. 4 is problematic due to the required modal transformations. Such transformations employ eigenvectors and -values of the system, resulting in an implicit dependency on the rotational speed Ω. However, it was discovered that the first 16 modal states of the system dominate its dynamic behavior up to approximately 800Hz. Therefore, truncating all higher modes does not affect the considered frequency range up to 400 Hz appreciably. In general, this approach is viable whenever the transformation of G by the right eigenvector-matrix of the standstill system, which does not result in a diagonal matrix, shows negligibly small cross-coupling between preserved and truncated modes. Otherwise, it might be necessary to keep more states than there are natural frequencies in the considered frequency band. In case of the system investigated in this paper, each the first four forward and backward whirl modes have to be preserved, as can be seen in fig. 3.

Unfortunately, an LTI formulation imposing the physical unbalances as model inputs is impossible, as unbalance forces exhibit a constant phase difference of 90° between x- and y-directions and an amplitude proportional to Ω^2. In particular, the unbalance forces $F_{U,i}$ are

$$F_{U,x} = U\Omega^2 \sin(\Omega t - \pi/2) \qquad F_{U,y} = U\Omega^2 \sin(\Omega t), \tag{3}$$

where U represents the unbalances and Ω the shaft's rotational speed, respectively. To overcome the issues mentioned above, the actual unbalances are substituted by force inputs at the disks. However, this simplification involves a loss of information regarding the unbalance characteristics or, more precisely, the exclusive excitation of forward whirl modes.

In summary, the model's inputs are discrete forces at the two disks as well as the voltages of the piezoelectric actuators, utilized as control inputs. Outputs are the x- and y-displacements at the disks, each measured by a sensor. Further in- and outputs have to be added for the LFT decomposition of the system, interconnecting the nominal system with the gyroscopic terms ΩG. For model validation and runup simulations, the test rig unbalances have been determined such that resonance vibration amplitudes in respective simulations and experimental runups match. Throughout this paper, the dynamics of electrical components, including time delays of the real time platform and anti-aliasing filters as well as phase lag of the power amplifiers driving the piezoelectric actuators, are neglected. The inclusion of these factors and subsequent real-time implementation of resulting controllers is currently being examined.

III. STRUCTURED SINGULAR VALUE SYNTHESIS

This section is used for a brief introduction on the Structured Singular Value introduced in [7], focusing on its applications to uncertain system analysis and synthesis of robust controllers, approached via SSV peak optimizations. For the following paragraphs, consider LTI systems with n in- and outputs, respectively. While all concepts shown here extend naturally to dynamics not being captured by square transfer matrices, this assumption makes the notation more compact. For imposing structured perturbations of the square transfer matrices at hand, consider the m-tuple

$$\begin{aligned}\mathcal{K}(m_r, m_c, m_C) = (&k_1, \ldots, k_{m_r}, k_{m_r+1}, \ldots, k_{m_r+m_c},\\ &k_{m_r+m_c+1}, \ldots, k_{m_r+m_c+m_C}),\end{aligned} \tag{4}$$

where

$$m = m_r + m_c + m_C \;\leq\; n, \tag{5}$$

$$\sum_{i=1}^{m} k_i = n. \tag{6}$$

The integers m_r, m_c, and m_C utilized in (4) and (5) account for the numbers of repeated real, repeated complex, and full complex perturbation elements, respectively. For $i \in \{1, \ldots, m\}$, each individual perturbation is a square block of size k_i. Therefore, the global, block-diagonal set of structured perturbations becomes

$$\begin{aligned}\mathbf{\Delta} := \big\{&\mathrm{diag}\left(\delta_1^r I_{k_1}, \ldots, \delta_{m_r}^r I_{k_{m_r}}, \delta_{m_r+1}^c I_{k_{m_r+1}}, \ldots,\right.\\ &\left.\delta_{m_r+m_c}^c I_{k_{m_r+m_c}}, \Delta_1^C, \ldots, \Delta_{m_C}^C\right):\\ &\delta_i^r \in \mathbb{R},\ \delta_i^c \in \mathbb{C},\ \Delta_i^C \in \mathbb{C}^{k_{m_r+m_c+i} \times k_{m_r+m_c+i}}\big\}.\end{aligned} \tag{7}$$

Notice that, employing straightforward in- and output conversions, any set of structured uncertainty composed of the three elements above can be transformed into block-diagonal form. For square transfer matrices and (4)-(7), the Structured Singular Value is defined as:

Definition 1, [35]: For $M \in \mathbb{C}^{n \times n}$, $\mu_{\mathbf{\Delta}}(M)$ is defined as

$$\mu_{\mathbf{\Delta}}(M) := \left(\min_{\Delta \in \mathbf{\Delta}} \{\bar{\sigma}(\Delta) : \det(I - M\Delta) = 0\}\right)^{-1} \tag{8}$$

unless no $\Delta \in \mathbf{\Delta}$ makes $I - M\Delta$ singular, in which case $\mu_{\mathbf{\Delta}}(M) := 0$.

That is, in terms of the $\mathcal{H}_\infty$-norm, the SSV is the reciprocal of the size of the smallest structured perturbation in $\mathbf{\Delta}$ destabilizing M. Conclusively, small values of μ at some particular frequency ω indicate high robustness with respect to some set of structured model perturbations at that frequency. Unfortunately, there exists no explicit solution to (8). In fact, it is shown in [4] that the exact computation of μ subject to real and mixed uncertainty sets $\mathbf{\Delta}$ is an NP-hard problem. Therefore, μ is usually approximated by pointwise upper and lower bounds across frequency. Such upper and lower bounds can be cast as scaled maximum singular value problems, the required scaling matrices being members of

the following sets [34]:

$$\mathcal{U}_{\mathcal{K}} := \Big\{ U \in \boldsymbol{\Delta} :\ \delta_i^r \in \left[\ -1 \quad 1\ \right],\ \delta_i^{c*}\delta_i^c = 1, \\ \Delta_i^{C*}\Delta_i^C = I_{k_{m_r+m_c+i}} \Big\} \tag{9}$$

$$\mathcal{D}_{\mathcal{K}} := \Big\{ \mathrm{diag}\left[D_1, \ldots, D_{m_r+m_c}, d_1 I_{k_{m_r+m_c+1}}, \ldots, d_{m_C} I_{k_m}\right] : \\ D_i \in \mathbb{C}^{k_i \times k_i},\ D_i = D_i^* > 0,\ d_j \in \mathbb{R},\ d_j > 0 \Big\} \tag{10}$$

$$\mathcal{G}_{\mathcal{K}} := \Big\{ \mathrm{diag}\left[G_1, \ldots, G_{m_r}, 0_{k_{m_1+1}}, \ldots, 0_{k_m}\right] : \\ D_i = D_i^* \in \mathbb{C}^{k_i \times k_i} \Big\} \tag{11}$$

Utilizing the above sets, a tight μ upper bound is [10]:

$$\beta_{\min} = \inf_{D\in\mathcal{D}_{\mathcal{K}}, G\in\mathcal{G}_{\mathcal{K}}} \inf_{\beta\in\mathbb{R}^+} \\ \left\{ \beta :\ \bar{\sigma}\left(\left(\frac{DMD^{-1}}{\beta} - jG \right) \left(I + G^2\right)^{-1/2} \right) \leq 1 \right\} \tag{12}$$

Including a lower bound based on the real spectral radius ρ_R, one obtains

$$\max_{U\in\mathcal{U}_{\mathcal{K}}} \rho_R\left(UM\right) \leq \mu_{\boldsymbol{\Delta}}\left(M\right) \leq \beta_{\min}. \tag{13}$$

For $m_r = 0$, the bounds in (13) simplify to

$$\max_{U\in\mathcal{U}_{\mathcal{K}}} \rho\left(UM\right) \leq \mu_{\boldsymbol{\Delta}}\left(M\right) \leq \inf_{D\in\mathcal{D}_{\mathcal{K}}} \bar{\sigma}\left(DMD^{-1}\right). \tag{14}$$

It turns out that the lower bounds with maxima in (13) and (14) are de facto equalities. However, it is common to use inequalities to account for the non-convexity of the underlying optimization problems, causing issues with local optima in the respective domains. In [19], a power method is suggested for approximating the complex μ lower bound problem in (14). This power algorithm is extended in [30] to tackle the mixed lower bound problem in (13). While the upper bounds in (13) and (14) are convex optimization problems that can be solved efficiently, they are not always equal to μ. Fortunately, the gaps between μ and its upper bounds tend to be small, making the upper bounds particularly useful for control synthesis. For the mixed case, that is $m_r > 0$, an alternative LMI upper bound is proposed in [31]. At the cost of increased computational effort, employing this LMI upper bound frequently results in tighter approximation of μ than solving the upper bound problem in (13). However, it seems LMI upper bounds have not yet been utilized directly for μ synthesis.

Minimizing the peak value of μ and thus optimizing the closed-loop robust performance with respect to $\boldsymbol{\Delta}$ across frequency is referred to as μ synthesis. That is, μ synthesis is equivalent to approaching a controller K_μ for a plant P such that

$$K_\mu = \arg\inf_K \sup_{\omega\in\mathbb{R}} \mu_{\boldsymbol{\Delta}}\left(\mathcal{F}_l\left(P, K\right)\right). \tag{15}$$

Anyway, as there is no explicit solution to computing μ, there also exists no explicit solution to this optimization. Hence, the μ synthesis problem is commonly approximated by minimizing the peak values of the upper bounds in (13) and (14), respectively. In order to penalize distinct performance measures, the plant model P in (15) is commonly augmented by diagonal, frequency-shaped weighting matrices W_i, including corresponding augmentation of $\boldsymbol{\Delta}$ with an unstructured performance block. Such augmentations of the μ synthesis setup (15) transform the optimization of robust stability under structured perturbations into an optimization of robust performance under structured perturbations, including the robust stability μ problem per definition. In general, the concept of augmenting LFT μ problems arises from the so-called Main Loop Theorem, omitted in this paper for convenience (see [9] or [35], for instance). For the remainder of this paper, the symbol $\boldsymbol{\mu_p}$ is used to indicate such robust performance μ upper bound problems.

A. Complex μ Synthesis

Approaching (15) for $m_r = 0$ is referred to as complex μ synthesis, the problem usually being approximated by minimizing the complex upper bound peak value in (14). Unfortunately, even after replacing μ by its upper bound, there is no closed-form solution to the resulting optimization problem. However, the upper bound problem can be effectively tackled by biconvex optimization over a controller K and the scaling matrices D in (14). This approach is the so-called D-K algorithm, first suggested in [8] and commercially accessible with the MATLAB Robust Control Toolbox™ (see [1], for instance).

D-K Iteration:

1) Find an initial estimate of the scaling matrices $\boldsymbol{D}\left(\omega\right)$ pointwise across frequency.
2) Find a state-space realization D fitting $\boldsymbol{D}\left(\omega\right)$, augment D such that

$$D_L := \mathrm{diag}\left[D, I_{n_y}\right],\ D_R := \mathrm{diag}\left[D^{-1}, I_{n_u}\right], \tag{16}$$

and construct the state-space system

$$P_D := D_L P D_R \tag{17}$$

so that by construction we have

$$\mathcal{F}_l\left(P_D, K\right) = D\mathcal{F}_l\left(P, K\right)D^{-1}. \tag{18}$$

3) Find $\hat{K}$ minimizing $\left\|\mathcal{F}_l\left(P_D, K\right)\right\|_\infty$ over all stabilizing, proper, real-rational controllers K.
4) Find pointwise scaling matrices $\hat{\boldsymbol{D}}\left(\omega\right)$ solving

$$\hat{\boldsymbol{D}}\left(\omega\right) = \arg\inf_{\boldsymbol{D}(\omega)\in\mathcal{D}_{\mathcal{K}}} \bar{\sigma} \\ \left(\boldsymbol{D}\left(\omega\right)\mathcal{F}_l\left(P, \hat{K}\right)\left(j\omega\right)\boldsymbol{D}^{-1}\left(\omega\right)\right). \tag{19}$$

5) Compare $\hat{\boldsymbol{D}}\left(\omega\right)$ with $\boldsymbol{D}\left(\omega\right)$. Stop if they are close, else replace $\boldsymbol{D}\left(\omega\right)$ with $\hat{\boldsymbol{D}}\left(\omega\right)$ and return to step 2.

It shall be mentioned at this point that the D-K algorithm is also frequently employed for tackling perturbation setups where $m_r > 0$, that is, mixed μ synthesis problems. While some - possibly large - degree of conservatism is induced by approximating the mixed by the complex upper bound problem, this approach has been applied to various synthesis setups in the past [17], [24].

B. Mixed μ Synthesis

There exist several approaches of extending the general idea of the D-K Iteration towards minimizing the upper bound in (14) for tackling mixed μ synthesis problems. The most common approach of approximating the mixed upper bound μ problem is the so-called (D,G)-K algorithm, posed in [32]. In analogy with the D-K algorithm, the (D,G)-K algorithm makes use of a biconvex optimization approach over a controller and the scaling matrices of the upper bound. However, due to the nature of (12), the biconvex approach is notably more involved than its complex counterpart. The (D,G)-K algorithm is available with the MATLAB Robust Control Toolbox™ and described comprehensively in [33].

An alternative to the (D,G)-K algorithm is the so-called μ-K Iteration suggested in [27]. Rather than directly extending the idea of the D-K algorithm to the mixed upper bound problem, the μ-K algorithm makes use of two layers of scaling matrices. In addition to the D-scales used within the D-K algorithm, the μ-K algorithm employs a scalar outer scale γ reflecting the ratio of mixed and complex upper bounds across frequency. That is, the μ-K algorithm's main idea is scaling D-K Iterations with respect to the frequency dependent degree of conservatism induced when employing the complex upper bound. While tending to produce slightly higher control orders than the (D,G)-K algorithm, the μ-K algorithm avoids state-space fits of the purely complex scaling matrices $G \in \mathcal{G}_{\mathcal{K}}$. In [28], the (D,G)-K and μ-K algorithms are appropriately distinguished as direct and indirect mixed upper bound minimizations, respectively.

Even though the μ-K algorithm appears to be a promising alternative for tackling mixed μ synthesis problems, it is not yet supported by commercially available software. Motivated by the synthesis of robust controllers for flexible high-speed rotors, the algorithm was implemented in MATLAB by the authors of this paper, using the iteration outline accessible in [28]. Furthermore, the algorithm has been extended by several means, permitting usage of the more accurate LMI upper bounds and internal order reductions, for instance. All augmentations of the algorithm including applications to particular control synthesis issues are addressed in [25].

IV. SYNTHESIS OF ROBUST CONTROLLERS

This section addresses augmentations of the nominal plant model described in section II such that both model perturbations and performance requirements are accounted for. The resulting perturbed open-loop model is then employed for synthesis of robust controllers.

A. Uncertainty Modeling

Appropriately accounting for model uncertainties is a crucial point in the scope of robust control. Though complex uncertainties in combination with the D-K algorithm produced some decent results for high-speed rotors, a significant degree of conservatism is going in hand with the complex uncertainty representations. Obviously, a more straightforward description of the speed-dependent dynamics is to define a real uncertain parameter Ω_u for the rotational speed, varying inbetween 0 and the peak operational speed of the shaft. An upper LFT of the speed-independent terms with the real matrix perturbation $-\Omega_u G$ captures all variations in the pointwise LTI dynamics. In combination with the real parametric uncertainty Ω_u, we make use of complex additive uncertainties Δ_a perturbing the outputs of $\mathcal{F}_u\left(P, -\Omega_u G\right)$, as shown in fig. 4. The additive, unstructured perturbations Δ_a are used to account for the decreasing model accuracy at high frequencies. The LFT diagram of the augmented, perturbed closed-loop system in fig. 4 additionally includes the diagonal scaling matrix W_z, described in further detail below.

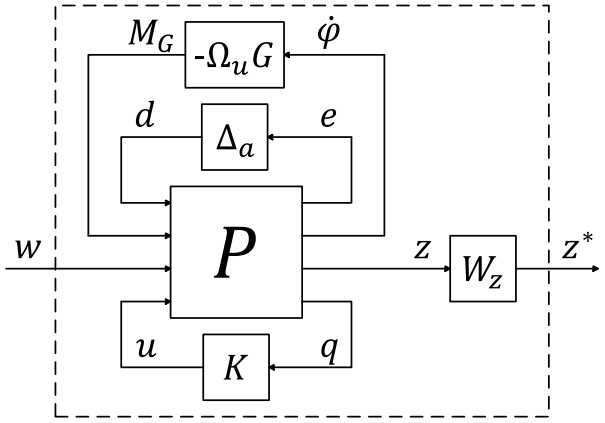

Fig. 4. Perturbed, augmented closed-loop system

Available literature on vibration control for flexible high-speed rotors avoids the plant description via real uncertain perturbations, presumably because Ω_u needs to be approximated with a complex parameter when approached via D-K iterations. When suitable algorithms for mixed perturbation setups are employed, the real uncertainty description of the speed-dependency tends to result in high computational effort and numerical issues [18]. Nevertheless, some publications employ the D-K algorithm ([17], [24]) to approach active vibration control for high-speed rotors. Other approaches for the consideration of gyroscopic effects stated in accessible literature utilize combinations of modal [2] and unstructured uncertainties [3]. Due to the implicit description of speed-dependencies, such approaches tend to introduce considerable conservatism, limiting their applicability and achievable performance results to a certain extent.

Due to the size of the gyroscopic matrix (16×16), an immediate implementation of the real parametric uncertainty-LFT for the reduced order plant model described in section II causes enormous numerical effort and could not be processed in reasonable time using μ-K and (D,G)-K algorithms. A step from FE to analytical modeling produces a solution: the inertias of the two disks are significantly larger than those of the remaining structure, suggesting that the latter elements can be neglected. Hence, it is sufficient to introduce only two in- and output channels per disk. For constant rotational speed Ω, the gyroscopic moments M_G around the x- and y-axes of a disk with polar moment of inertia Θ are calculated

using the disk's angular velocities $\dot{\varphi}_i$:

$$\begin{bmatrix} M_{G,x} \\ M_{G,y} \end{bmatrix} = \Omega \begin{bmatrix} 0 & \Theta \\ -\Theta & 0 \end{bmatrix} \begin{bmatrix} \dot{\varphi}_x \\ \dot{\varphi}_y \end{bmatrix} \tag{20}$$

By this setup, G can be reduced to an order of four, allowing for mixed μ synthesis at reasonable computational effort.

B. Performance Measures

Preceding control synthesis, the perturbed plant model is augmented for improved performance measures regarding unbalance vibrations. As indicated in section II, the plant inputs do not contain the appropriate characteristics of the actual unbalance excitations, but local force inputs at the disks. As unbalances do not excite backward whirl modes, efficient performance measures should not highlight gains corresponding to such modes. Otherwise, significant conservatism might be induced, limiting the achievable reduction of forward whirl vibrations.

Intuitively, one might attempt defining closed-loop vibration bounds penalizing high gains at forward whirl frequencies heavier than such in the proximity of backward whirl frequencies. For actual rotor systems, however, the utilization of such setups is not straightforward as both forward and backward whirl modes start at the same natural frequency at standstill. That is, a bound being loose at backward whirl frequencies and tight at forward whirl frequencies would require a large order, subsequently raising the order of the augmented plant. This might, in turn, increase both likelihood of numerical problems and computational effort, respectively. Furthermore, backward whirl frequencies intersect with forward whirls of other modes at certain rotational speeds. Therefore, we propose an adaptation of the model instead of the performance measures. Based on the disk's vibration outputs, additional outputs are generated via modal scaling. For that purpose, the nominal plant model is transformed into modal form, providing access to the respective influences of individual modes on the plant outputs. In modal state-space representations, the i-th column of the output matrix $\tilde{C}$ accounts the impact of the i-th modal state on the output vector:

$$\dot{\tilde{x}} = \tilde{A}\tilde{x} + \tilde{B}u \qquad y = \tilde{C}\tilde{x} \tag{21}$$

Utilizing a modal state-space representation (21), the undesired backward whirl modes can be eliminated for performance assessment by simply replacing the corresponding elements of $\tilde{C}$ with zeros. To avoid excitation of backward whirls by the controller, though, a scaling factor $\alpha << 1$ is imposed instead. Even though the transformation to (21) depends on the rotational speed Ω and some decoupling of the modal states $\tilde{x}$ is lost due to the LFT between speed-dependent and -independent terms (see fig. 4), this semi-modal performance approach works very well for the system at hand. Performance assessment after modal elimination of backward whirl influence from the output vector matches the requirement of reducing unbalance excitation at significantly less conservatism than the use of true displacements.

Ultimately, the augmented plant model displayed in fig. 4 enables two choices of performance measures z, physical displacement signals and such after elimination of backward whirl influence, respectively. In either case, closed-loop bounds in the sense of $\mathcal{H}_\infty$-norm performance assessment are imposed using a diagonal scaling matrix W_z such that $z^* = W_z z$. The particular choice of closed-loop bounds restricts the chosen displacements signals in the proximity of the first forward whirl mode at disk one and the second one at disk two, respectively. This spatial performance assessment allows penalizing the two forward whirl modes within operating range almost independently, as the first forward whirl mode has more influence on disk one and the second on disk two. Notice that without modal elimination of backward whirl modes, each of the two closed-loop signal bounds also penalizes the corresponding backward whirls. It is shown in table I and section V how the conservatism induced by penalizing backward whirl modes notably limits the achievable closed-loop performance. Transfer functions for random, bounded perturbations including the closed-loop signal bounds (dashed) are displayed for the initial system behavior in fig. 5 and after modal backward whirl elimination (BWE) in fig. 6.

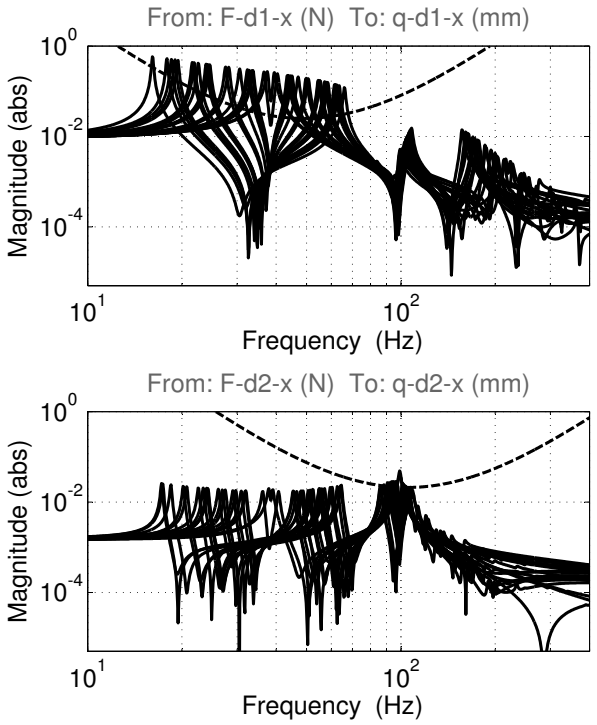

Fig. 5. Synthesis setup: perturbed system without backward whirl elimination (solid), closed-loop bound (dashed)

C. Robust Control

The reduction in conservatism achieved when treating Ω_u as a real parametric uncertainty is indicated by the μ upper bound peaks of the augmented plant model. These μ peaks are included in table I, the index p referring to robust *performance*, while the superscripts c and m distinguish purely *complex* and *mixed* perturbation models, respectively. The ratios between $\boldsymbol{\mu_p^c}$ and $\boldsymbol{\mu_p^m}$ for the particular augmented open- and closed-loop systems indicate the significant conservatism

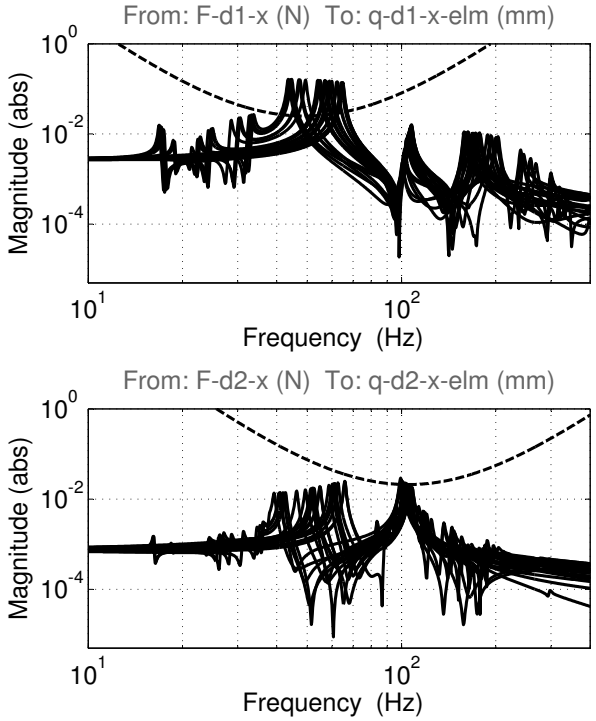

Fig. 6. Synthesis setup: perturbed system after backward whirl elimination (solid), closed-loop bound (dashed)

associated with approximating bounded, varying rotational speeds by a complex perturbation elements. Furthermore, the final column of table I (i.e., $\boldsymbol{\mu_p^m}$) strongly reflects the conservatism induced when utilizing the performance setup without backward whirl elimination (BWE, recall fig. 5) from the displacement outputs. That is, for each pair of values for $\boldsymbol{\mu_p^m}$, the one without BWE is notably higher.

TABLE I
SSV BOUND PEAK VALUES

Type	BWE	Order	$\boldsymbol{\mu_p^c}$	$\boldsymbol{\mu_p^m}$
Aug. Plant	y	-	53.21	13.03
	n	-	62.20	14.56
$\mathcal{H}_\infty$	y	68	40.82	8.73
	n	68	40.81	9.87
D-K	y	68	40.82	8.73
	n	116	40.77	11.78
IR μ-K	y	77	13.87	1.08
	n	48	12.73	1.51

The μ peaks of the $\mathcal{H}_\infty$ controllers indicate how unstructured perturbations approximating (4)-(7) are not appropriate to address the perturbations of the system at hand. In fact, the two $\mathcal{H}_\infty$ controllers merely improve the robust performance of the augmented plant model. Similar results have been obtained using the D-K algorithm, approximating (4)-(7) by a purely complex perturbation structure and inherently optimizing $\boldsymbol{\mu_p^c} \geq \boldsymbol{\mu_p^m}$. As the D-K iteration implicitly attempts stabilizing the dynamics subject to complex perturbations, it does not produce a controller better than the $\mathcal{H}_\infty$ controller used to initialize the algorithm. In fact, the improved value $\boldsymbol{\mu_p^c}$ for the performance setup without backward whirl elimination (BWE) goes in hand with a raise in $\boldsymbol{\mu_p^m}$ and, conclusively, an actual decrease in robust performance.

As expected, the real parametric uncertainty description of the plant's speed-dependency in combination with appropriate algorithms allows for significantly better results. In particular, the augmented μ-K algorithm including internal order reduction (IR) of the controllers at each iteration in combination with the utilization of LMI bounds achieved superb results. Notice that table I does not include μ peaks for (D,G)-K controllers due to numerical issues similar to those reported in the literature [18]. Anyhow, the results achieved using the augmented μ-K algorithm for explicit treatment of mixed perturbations and the inclusion of semi-modal performance measures are highly promising.

V. CLOSED-LOOP RESULTS

In order to display the perceptible performance for the test rig, unbalance simulations are performed. Fig. 7 shows simulated steady-state unbalance vibration amplitudes at disks 1 and 2 in x-direction, caused by a quasi-stationary runup. Due to the almost symmetric closed-loop behavior, y-directions have been omitted. Within all simulations, the maximum voltages are slightly above 300 V, which is clearly below the maximum amplifier voltage at 500 V, so that no further bounding of the control input signals was necessary. The simulated unbalances are those identified for the test rig, publications regarding alternative control schemes applied to the same test rig indicating that such simulations are suitable for capturing the actual system behavior [22], [23].

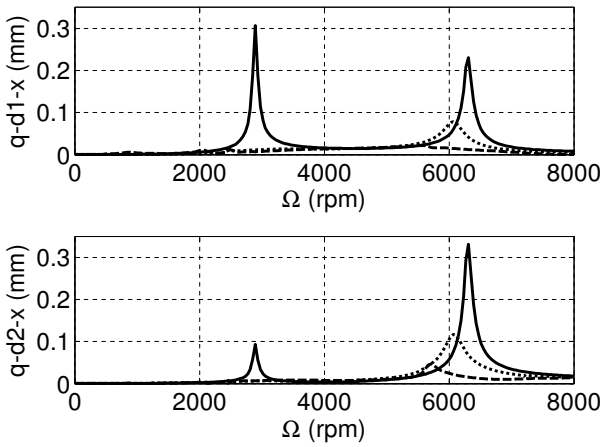

Fig. 7. Quasi-stationary runup simulation for unbalance excitation: open-loop plant (solid), closed-loop using IR μ-K controller without BWE (dotted), closed-loop using IR μ-K controller including BWE (dashed)

Corresponding to the achieved peak μ values, the internal reduction (IR) μ-K controllers yield significant vibration reduction. Comparing both IR μ-K controllers, the one designed at the hand of the BWE system achieves remarkably

more reduction than the one designed using physical performance outputs. The D-K and $\mathcal{H}_\infty$ controllers do not reduce the resonance amplitudes of the passive system. Although table I shows decreased μ peaks for the corresponding controllers. This indicates that, even though the open-loop plant is robustly stable, the complex stability problem dominates the complex performance problem. Once more, these results demonstrate how complex uncertainty sets are particularly more conservative than mixed perturbation setups whenever severe levels of gyroscopic effects are present.

VI. CONCLUSIONS

We have proposed an efficient framework of synthesizing robust controllers for flexible high-speed rotors subject to severe gyroscopic effects via mixed μ synthesis. Employing real parametric uncertainties, the speed-dependency of the system dynamics is appropriately accounted for, whereas the degree of model-induced conservatism is notably low. In combination with semi-modal performance measures, allowing penalties on individual modes, remarkable closed-loop results were shown. In particular, the extended μ-K algorithm, incorporating internal order reductions and LMI μ bounds, achieved great attenuation of bending vibrations. Future research directions include extensions regarding time delays, noise sensitivity, control order reduction, and the subsequent test rig implementation.

REFERENCES

[1] G.J. Balas, R. Chiang, A. Packard, and M. Safonov, Robust Control Toolbox: Getting Started Guide, The MathWorks, Inc., R2012a edition, 2012.

[2] G.J. Balas and P.M. Young, Control Design for Variations in Structural Natural Frequencies, Journal of Guidance, Control, and Dynamics, Vol. 18, No. 2, Pp. 325-332, 1995.

[3] H.M.N.K. Balini, C.W. Scherer, and J. Witte, Performance Enhancement for AMB Systems Using Unstable $\mathcal{H}_\infty$ Controllers, IEEE Transactions on Control Systems Technology, Vol. 19, No. 6, Pp. 1-15, 2011.

[4] R.P. Braatz, P.M. Young, J.C. Doyle, and M. Morari, Computational Complexity of μ Calculation, Automatic Control, IEEE Transactions on, Vol. 39, No. 5, Pp. 1000-1002, 1994.

[5] C.R. Burrows, M.N. Sahinkaya, and O.S. Turkay, An Adaptive Squeeze-Film Bearing, ASME Journal of Tribology, Vol. 106, Pp. 145-151, 1984.

[6] Y. Chen and C. Zhu, Active Vibration Control Based on Linear Matrix Inequality for Rotor System under Seismic Excitation, Journal of Sound and Vibration, Vol. 314, No. 1-2, Pp. 53-69, 2008.

[7] J.C. Doyle, Analysis of Feedback Systems with Structured Uncertainties, Control Theory and Applications, IEE Proceedings D, Vol. 129, No. 6, Pp. 242-250, 1982

[8] J.C. Doyle, Synthesis of Robust Controllers and Filters, In Decision and Control, The 22nd IEEE Conference on, 1983, Vol. 22, Pp. 109-14, 1983.

[9] J.C. Doyle, A.K. Packard, and K. Zhou, Review of LFTs, LMIs, and μ, In Decision and Control, Proceedings of the 30th IEEE Conference on, Vol.2, Pp. 1227-1232, 1991.

[10] M.K.H. Fan, A.L. Tits, and J.C. Doyle, Robustness in the Presence of Mixed Parametric Uncertainty and Unmodeled Dynamics, Automatic Control, IEEE Transactions on, Vol. 36, No. 1, Pp. 25-38, 1991.

[11] R.L. Fittro and C.R. Knospe, Rotor Compliance Minimization Via μ-Control of Active Magnetic Bearings, IEEE Transactions on Control Systems Technology, Vol. 10, No. 2, Pp. 238-249, 2002.

[12] R. Gasch, R. Nordmann, and H. Pfuetzner, Rotordynamik, Springer Verlag, Berlin, Germany, 2006.

[13] H. Gibson, $\mathcal{H}_\infty$ Control of Active Magnetic Bearings: An Intelligent Uncertainty Modeling Approach, PhD Thesis, North Carolina State University, Raleigh (NC), USA, 2004.

[14] T. Ikeda, Fundamentals of Piezoelectricity, Oxford University Press, USA, 1997

[15] M.E. Johnson, L.P. Nascimento, M. Kasarda, and C.R. Fuller, The Effect of Actuator and Sensor Placement on the Active Control of Rotor Unbalance, Journal of Vibration and Acoustics, Vol. 125, Pp. 365-373, 2003.

[16] S. Kern, Increasing Process Stability of Milling Spindles by Active Damping by means of Electromagnetic Actuators, PhD Thesis (in German), TU Darmstadt, Darmstadt, Germany, 2008.

[17] A. Lanzon and P. Tsiotras, A Combined Application of $\mathcal{H}_\infty$ Loop Shaping and μ-Synthesis to Control High-Speed Flywheels, IEEE Transactions on Control Systems Technology, Vol. 13, No. 5, Pp. 766-777, 2005.

[18] G. Li, Z. Lin, P.E. Allaire, et al., Stabilization of a High Speed Rotor with Active Magnetic Bearings by a Piecewise μ-Synthesis Controller, 6th Symposium on Magnetic Suspension Technology, Turin, Italy, 2001.

[19] A.K. Packard, M.K.H. Fan and J.C. Doyle, A Power Method for the Structured Singular Value, Proc. of the 1988 IEEE Conference on Control and Decision, Pp. 2132-2137, 1988.

[20] A.B. Palazzolo, R.R. Lin, R.M. Alexander, A.F. Kascak, and J. Montague, Test and Theory for Piezoelectric Actuator-Active Vibration Control of Rotating Machinery, Journal of Vibration, Acoustics, Stress, and Reliability in Design, Vol. 113, No. 2, Pp. 167-175, 1991.

[21] B. Riemann, E.A. Perini, K. Lucchesi-Cavalca, H. Fiori de Castro, and S. Rinderknecht, Oil Whip Instability Control Using μ-Synthesis Technique on a Magnetic Actuator, Journal of Sound and Vibration, Vol. 332, No. 4, Pp. 654-673, 2013.

[22] Z. Wang, R.S. Schittenhelm, M. Borsdorf, and S. Rinderknecht, Application of Augmented Observer for Fault Diagnosis in Rotor Systems, Engineering Letters, Vol. 21, No. 1, Pp. 10-17, 2013

[23] R.S. Schittenhelm, B. Riemann, and S. Rinderknecht, Active Vibration Control for a Rotor System Subject to Gyroscopic Effects using the FxLMS-Algorithm (in German), Vibrations in Rotating Machines, Berlin, 2013.

[24] U. Schoenhoff, Practical Robust Control of Mechatronic Systems with Structural Flexibilities, PhD Thesis, TU Darmstadt, Darmstadt, Germany, 2003.

[25] M. Sehr, Synthesis of Robust Controllers for Mixed Uncertainties via μ-K Iteration, M.Sc. thesis, Dept. Mechanical Engineering, TU Darmstadt, Germany, 2012.

[26] M.S. Senousy, R.K.N.D. Rajapakse, and M.S. Gadala, Self-Heat Generation in Piezoelectric Stack Actuators used in Fuel Injectors, Smart Materials and Structures, Vol. 18, No. 4, 2009.

[27] S. Toeffner-Clausen, P. Andersen, J. Stoustrup, and H.H. Niemann, A New Approach to μ-Synthesis for Mixed Perturbation Sets, In Proceedings of the 3rd European Control Conference, ECC95, Pp. 147-152, 1995.

[28] S. Toeffner-Clausen, System Identification and Robust Control: A Case Study Approach, Springer London, 1996.

[29] K. Youcef-Toumi and S. Reddy, Dynamic Analysis and Control of High Speed and High Precision Active Magnetic Bearings, Journal of Dynamic Systems, Measurement and Control, Transactions of the ASME, Vol. 114, No. 4, Pp. 623-633, 1992.

[30] P.M. Young and J.C. Doyle, Computation of μ with Real and Complex Uncertainties, Proceedings of the 29th IEEE Conference on Decision and Control, Pp. 1230-1235, 1990.

[31] P.M. Young, M.P. Newlin, and J.C. Doyle, Practical Computation of the Mixed μ Problem, Proceedings of the American Control Conference, Pp. 2190-2194, 1992.

[32] P.M. Young, Controller Design with Mixed Uncertainties, In American Control Conference, Vol. 2, Pp. 2333-2337, 1994.

[33] P.M. Young, Controller Design with Real Parametric Uncertainty, International Journal of Control, Vol. 65, No. 3, Pp. 469-509, 1996.

[34] P.M. Young, Structured Singular Value Approach for Systems with Parametric Uncertainty, International Journal of Robust and Nonlinear Control, Vol. 11 No. 7, Pp. 653-680, 2001.

[35] K. Zhou, J.C. Doyle, and K. Glover, Robust and Optimal Control, Prentice Hall, 1996.

[36] K. Zhou, Frequency-Weighted Model Reduction with $\mathcal{L}_\infty$ Error Bounds, Systems & Control Letters, Vol. 21, 115-125, 1993.